ELSEVIER

Food Chemistry 51 (1994) 349–357

0308-8146/94/$7.00

The formation and growth of carbon dioxide gas bubbles from supersaturated aqueous solutions

M. J. Hey, A. M. Hilton

Department of Chemistry, University of Nottingham, Nottingham, UK, NG7 2RD

&

R. D. Bee

Unilever Research, Colworth House, Sharnbrook, Bedford, UK, MK44 1LQ

A simple stopped-flow apparatus has been devised to follow the growth of gas bubbles formed after the rapid establishment of a supersaturated aqueous carbon dioxide solution by the reaction of hydrogen ions with bicarbonate ions. Turbidimetric measurements taken over a period of *c.*200 ms, supplemented by analysis of photographic and videotape recordings at later times have shown that bubble growth is a diffusion-limited process. Experimental results obtained with a hydrophobised cell led to the conclusion that at supersaturations typical of carbonated beverages the mechanism of bubble formation probably involves pre-existing gas cells trapped on the surface. Adsorption of sodium dodecyl sulphate, β-casein or β-lactoglobulin onto the hydrophobic surface reduced the number of bubbles, but solutions of sodium dodecyl sulphate above the critical micelle concentration produced additional bubbles.

INTRODUCTION

Bubble release from aqueous solutions which are supersaturated with respect to dissolved carbon dioxide is of obvious interest in the production of carbonated beverages. The number and size of the bubbles formed are influenced by factors such as the degree of supersaturation, solution viscosity and the addition of surface-active agents. In order to study the effect of these and other factors, most previous experimental work has involved saturating a solution under a high pressure of gas and then rapidly releasing the pressure to produce supersaturation (e.g. Lubetkin, 1989). In this paper, data are presented which were obtained from experiments in which supersaturation was achieved by the rapid chemical formation of carbon dioxide *in situ*. A preliminary report of some of these results has already been published (Hilton *et al.*, 1993).

In aqueous solution, carbon dioxide can be rapidly generated by the reaction of hydrogen ions with bicarbonate ions

$$H^+ + HCO_3^- \rightarrow CO_2(aq) + H_2O$$

At 25°C and an ionic strength of 0·055 mol dm^{-3} the second-order rate constant is 5·5 × 10^4 dm^3 mol^{-1} s^{-1} (Gibbons & Edsall, 1963). For reagent concentrations of 0·1 mol dm^{-3}, therefore, the half-life of the reaction will be of the order of 10^{-4}s and reaction will be essentially complete before gas bubbles begin to form. Supersaturations can thus be readily controlled by choosing appropriate initial concentrations for the reagents. To achieve rapid mixing of the reagent solutions, a simple stopped flow apparatus has been constructed. Bubble growth was monitored turbidimetrically over an interval of *c.*200 ms following mixing and by videophotography after that. The number of bubbles in the reaction cell was recorded photographically.

MATERIALS AND METHODS

Stopped flow apparatus

Gas bubbles were generated in the cylindrical glass reaction cell (internal dimensions: length 8·28 cm, diameter 0·38 cm) of the stopped flow apparatus shown diagrammatically in Fig. 1. Equal volumes (2 cm^3) of equimolar hydrochloric acid and sodium bicarbonate solutions were expelled from two identical syringes into the reaction cell by pushing the syringe pistons forward in unison with a driving plate. When the pistons

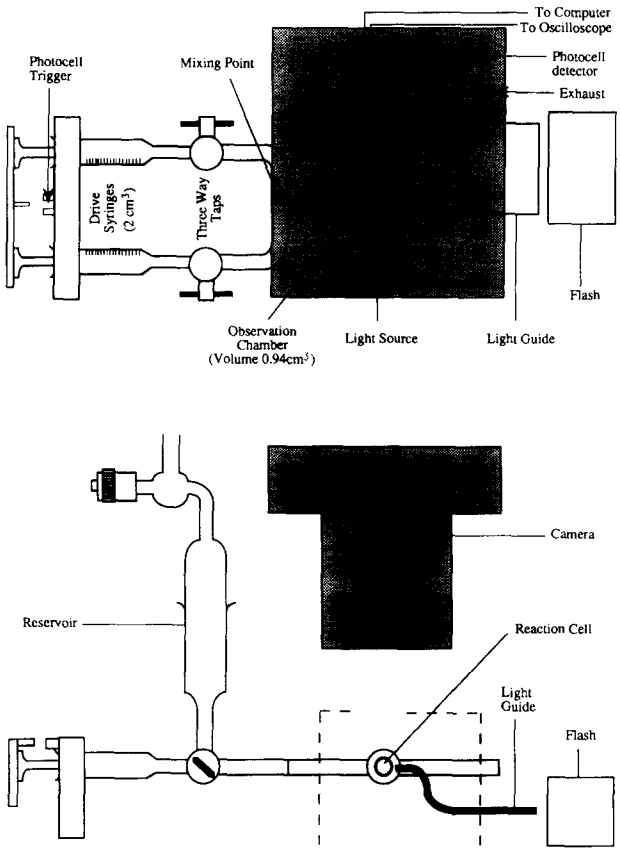

Fig. 1. A schematic diagram of the stopped-flow apparatus (from Hilton *et al.* , with permission).

reached the end of their travel, the flow of liquid through the cell stopped and a small vane attached to the driving plate interrupted a light beam to trigger a flash gun and the shutter of an Olympus OM-2 camera which was mounted directly above the reaction cell. The delay between the trigger signal and the opening of the shutter was measured and found to be 130 ± 5 ms. A Quantimet 970 Image Analyser (Cambridge Instruments) was used to obtain bubble sizes from images read directly from 35-mm film negatives placed on the stage of a microscope, using low power magnification. Lead shot of known diameter were photographed in the cell to check that the images were not distorted or magnified by the cell walls. Video recordings made of the later stages of bubble growth were viewed and edited on a television monitor. Photographs of frames displayed on the monitor screen were used in conjunction with a Zeiss Particle Sizer (TGA 10) to estimate bubble sizes at intervals of 0·2 s.

In order to monitor solution turbidity, a tungsten filament lamp was positioned so that a light beam passed along the axis of the cell to fall onto a sensitive, high area, fast response photovoltaic detector (RS 303-674). A zero control applied a backing voltage to offset the signal level when the reaction cell was filled with bubble-free solution. After amplification, the difference signal resulting from the scattering of light by bubbles in the cell went to the analogue input of a BBC Model B microcomputer (Acorn) where analogue-to-digital conversion was started by the trigger signal. Turbidities were calculated as a function of elapsed time (t) after the trigger signal according to the equation

$$\tau = \frac{\ln(V_0/V)}{l} \qquad (1)$$

where V is the voltage recorded at time t, V_0 is the initial voltage and l is the internal cell length.

For some experiments the reaction cell was hydrophobised by filling it with a solution of a perfluorinated acrylate polymer (FC723,3M) dissolved in a perfluorinated hydrocarbon solvent (Freon 113,3M). Adsorption of the polymer onto the cell surface for 1 h produced an extremely thin, hydrophobic film as shown by scanning electron microscopy (JEOL JSM 35C) and contact-angle measurements carried out on glass microscope slides treated in the same way. The adsorbed polymer layer could be removed by treatment with a mixture of Freon 113 and methanolic sodium hydroxide solution. Protein-covered surfaces were prepared by soaking the hydrophobised reaction cell for 3 h with sodium phosphate solutions of β-lactoglobulin (Sigma) or β-casein (90%; Sigma) buffered at pH 8·9 after the surface had been preconditioned by leaving the cell filled overnight with the buffer solution. Protein concentrations of 1·0 mg cm^{-3} were used to ensure saturation coverage of the surface (Luey *et al.*, 1991).

Preparation of solutions

Aqueous solutions of AnalaR grade reagents were made up with de-ionised water which had been triple-distilled in an all-glass apparatus. Glassware, including the stopped flow apparatus, was cleaned by soaking in concentrated nitric acid for 24 h followed by copious rinsing with purified water. Stock solutions were sonicated to ensure complete mixing and then filtered under pressure through 0·22-μm membrane filters (Millipore) to remove dust particles. Before use in the stopped flow apparatus all solutions were thermostatted at 25°C in a water bath for a minimum of 1 h.

Some solutions were prepared by dissolving the reagents in water containing 25% (v/v) glycerol. Relative viscosities of solutions of NaCl in water and in the glycerol/water mixed solvent were determined at 25°C with an Ostwald viscometer, using purified water as a reference standard. An allowance was made for the effect on efflux times of differing solution densities.

Carbon dioxide solubility

The solubilities of CO_2 at 25°C in water and in aqueous NaCl solutions corresponding to those produced by the hydrochloric acid–sodium bicarbonate reaction were determined by introducing gas at a known initial pressure into commercial aerosol cans containing measured

volumes of solution. After vigorous shaking to equilibrate the gas/liquid mixture, the final gas pressure was recorded by a transducer. The mass of CO_2 dissolved in the solution at the final pressure was calculated on the assumption that the gas behaved ideally. For an equilibrium pressure of 1 atmosphere of CO_2, the concentration of dissolved gas was calculated as 0·035 mol dm^{-3} in water compared to 0·034 mol dm^{-3} from published data (Fogg & Gerrard, 1991) and 0·025 mol dm^{-3} in 25% aqueous glycerol. In salt solutions, a reduction of approximately 20% was observed in CO_2 solubility as the NaCl concentration was increased to 0·50 mol dm^{-3}. The results of these experiments were used as a basis for quoting supersaturation ratios.

Surface tensions

The apparatus constructed to measure the surface tensions of sodium dodecyl sulphate (SDS) solutions was based on the dual capillary modification of the maximum bubble pressure method (Sugden, 1924). Two glass capillaries of tip radii 0·11145 and 0·00972 cm respectively were immersed in a test solution to the same depth and the difference in pressure required to liberate CO_2 bubbles from the two tips determined. A manometer containing a diffusion pump oil (Apiezon B) and thermostatted at 25°C by a water jacket was read with a travelling microscope. Surface tensions were calculated from the Young–Laplace equation.

Contact angles

Advancing and receding contact angles were measured for liquid drops placed on glass microscope slides which had been treated and cleaned in an identical procedure to that used for the stopped flow apparatus. The equipment consisted of a telescope fitted with a goniometer, sample platform, adjustable wedge and filament lamp. Microscope slides supported on the sample platform were mounted on the adjustable wedge which could be tilted at a variable angle to the horizontal. After deposition of a drop on a slide in the horizontal position, the angle of tilt was adjusted to produce a distortion of the drop shape. The illuminated profile of the drop in a plane normal to the axis of rotation of the wedge was then viewed with the telescope. Crosswires in the eyepiece used in conjunction with the goniometer allowed the contact angles at the leading and trailing edges of the drop to be measured as a function of the tilt angle.

RESULTS AND DISCUSSION

Bubble growth

The intensity of a light beam passing through a non-absorbing suspension of bubbles is attenuated by the scattering which takes place at the liquid/gas interfaces. The turbidity τ of the suspension is defined by the equation

$$I = I_0 \exp(-\tau l) \tag{2}$$

where I and I_0 are the transmitted and incident light intensities respectively of a light beam of path length l. A monodisperse suspension containing N bubbles/unit volume has a turbidity given by

$$\tau = NC \tag{3}$$

where C is the bubble scattering cross-section. For spherical bubbles of radius r, C is related to the geometric cross-section by an efficiency factor such that

$$C = Q\pi r^2 \tag{4}$$

The value of Q which ranges from near 0 to about 5 depends on the refractive index of the solution, the ratio of the bubble radius to the wavelength of the light in the liquid and the solid angles subtended by the beams of incident and measured radiation. Theoretical treatment is simplest if an incident parallel beam of zero angle is assumed and if the receiving device also subtends zero angle at the scattering particles, when, for example, Q approaches 2 for bubbles large compared to the wavelength of the light and small compared to the cross-sectional area of the beam. However since beams of zero angle are never realized in practice and the apparent values of Q will be reduced below the theoretical values, Lothian and Chappel (1951) recommend that when turbidity measurements are used to estimate particle sizes, the relevant value of Q should be determined experimentally with the particular conditions of apparatus and particle to be used.

Some typical turbidimetric data are shown in Fig. 2 in which the turbidities are divided by the number of bubbles/unit volume at 130 ms after mixing of the reagents. The linearity of plots of τ/N versus time for different initial CO_2 concentrations suggests that N remains constant over the measurement period, implying that bubble formation occurs in a short burst in the first few milliseconds following establishment of supersaturation. Hence the change in τ/N can be interpreted as a constant rate of increase in the scattering cross-section of a growing bubble, i.e. $r^2 \propto t$. This relationship is characteristic of a diffusion-controlled process and has been observed in a study of the growth rates of microscopic air bubbles resting underneath a Perspex plate in supersaturated water (Manley, 1960).

Figure 3 shows how the rate of change of τ/N depends on initial CO_2 concentration. An approximately linear relationship is evident. To confirm that a diffusion-limited rate process was occurring during bubble growth, rates were re-measured in the presence of added glycerol. The results presented in Fig. 3 show that when the viscosities of the reagent solutions were doubled by the addition of 25% (v/v) glycerol, the rates decreased by a factor of 4–5. Since the scattering effi-

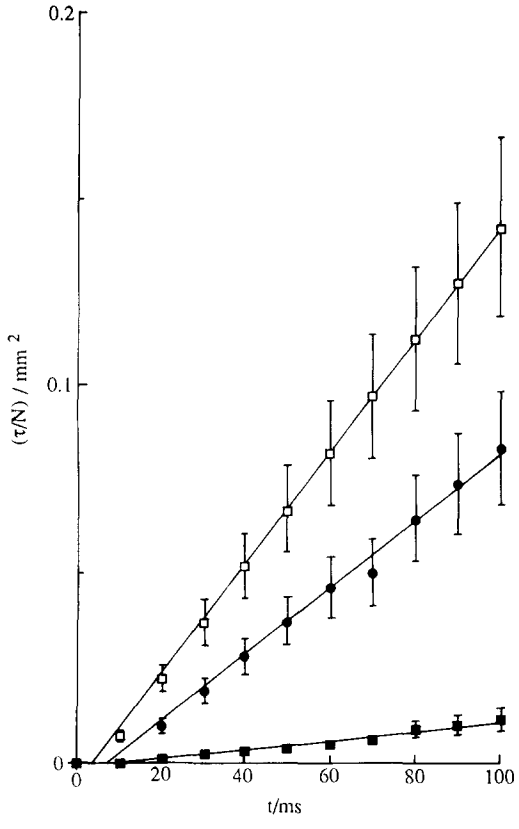

Fig. 2. Increase in turbidity normalised with respect to number of CO_2 gas bubbles/unit volume of solution following establishment of supersaturation. Initial CO_2 concentrations: (■) 0·15, (●) 0·30 and (□) 0·50 mol dm^{-3}. Error bars are estimated from the standard deviations in mean values of N.

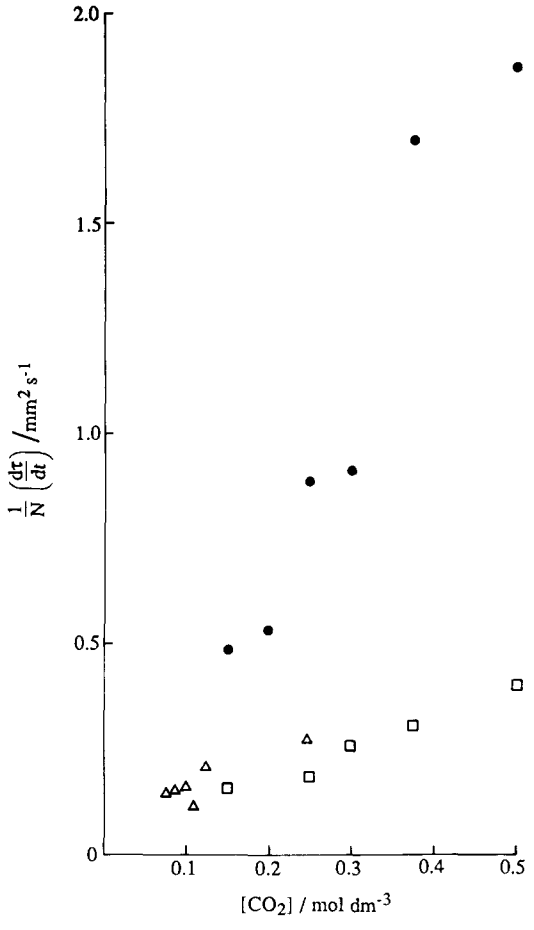

Fig. 3. Rates of increase of normalised turbidities plotted as a function of initial CO_2 concentration: (●) untreated cell, (□) untreated cell + 25% added glycerol, (Δ) hydrophobised cell + 25% added glycerol.

ciency factor Q may also change in the glycerol solutions, this reduction factor may not be correct for rates expressed in terms of the geometric cross-sections; nevertheless the decrease is of the order of magnitude expected for a reduction in the CO_2 diffusion coefficient. Figure 3 also includes data obtained from a hydrophobised cell. Although many more bubbles were produced for a given CO_2 concentration so that the turbidity increased much faster than in the untreated cell, the rates of increase of τ/N were similar in the two cells.

The problem of calculating the rate at which gas bubbles either dissolve or grow in undersaturated or supersaturated solutions respectively has been considered by Epstein and Plesset (1950) who used a 'quasi-stationary' model in which convective transport terms are neglected. In their simplest model these authors also ignored the surface tension of the bubble boundary, since its inclusion generally means that valid analytical solutions cannot be obtained. Later numerical calculations, however, predict that growth rates in supersaturated solutions which are inhibited initially by surface tension do achieve the analytical asymptotic regime for growth ignoring surface tension (Cable & Frade, 1988).

The result of solving the diffusion equation for these conditions is to obtain a time-dependent expression for the concentration gradient around the bubble. Further simplification can be achieved by assuming that a steady-state gradient is reached, when the equation for the growth rate becomes

$$\frac{dr}{dt} = \frac{D(c_i - c_s)}{\rho r} \tag{5}$$

where D is the diffusion coefficient of gas molecules in solution, c_i is the concentration of dissolved gas, c_s is the concentration in a saturated solution and ρ is the gas density in the bubble. Integration of eqn (5) with $r = r_0$ at $t = 0$ gives

$$r^2 = r_0^2 + \frac{2D(c_i - c_s)t}{\rho} \tag{6}$$

Equation (6) can be combined with eqns (3) and (4) to give the time dependence of the turbidity of a suspension of growing bubbles

$$\frac{\tau}{N} = \left(\frac{\tau}{N}\right)_0 + k(c_i - c_s)t \tag{7}$$

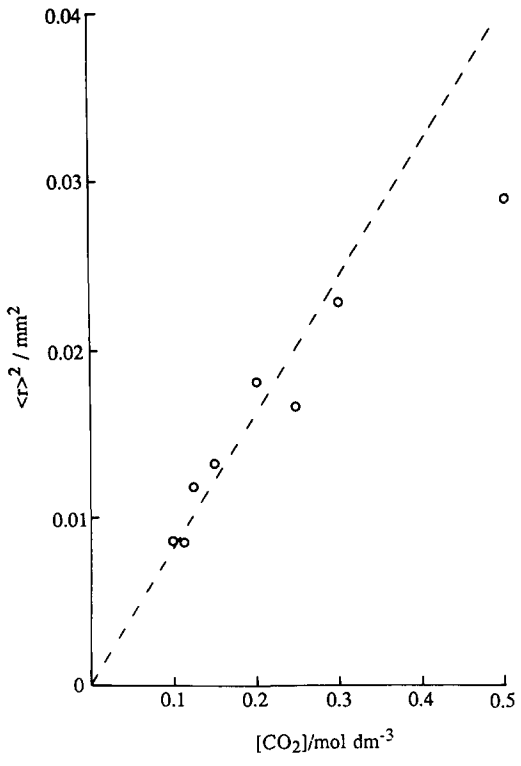

Fig. 4. Mean square bubble radius at t = 130 ms as a function of initial CO_2 concentration.

where $k = 2\pi QD/\rho$. In view of the approximate nature of the analytical solution to the diffusion equation however, it is more realistic to write $k = Qg$ and to regard g, the rate of increase of the geometric cross-sectional area normalised with respect to $(c_i - c_s)$, as an empirical parameter.

The gradients of the plots in Fig. 3 give values for k of approximately 4×10^{-9} and 1×10^{-9} m^5 mol^{-1} s^{-1} for the aqueous and glycerol-containing solutions respectively. Bubble size data obtained from image analysis of photographs of the glycerol-containing solutions at t = 130 ms after mixing are shown in Fig. 4. For each CO_2 concentration, more than 100 bubbles were sized to obtain a surface-averaged radius. A plot of the square of the mean bubble radius against CO_2 concentration is linear, in accordance with eqn (6), for gas concentrations less than about 0·25 mol dm^{-3}. The gradient of 8×10^{-11} m^5 mol^{-1} corresponds to a value for g of $1{\cdot}9 \times 10^{-9}$ m^5 mol^{-1} s^{-1} which when combined with the turbidity data leads to a scattering efficiency factor of 0·5 in the glycerol solutions.

Video images of bubbles recorded up to 1 s after formation allowed a direct estimation of their growth rates to be made. In Fig. 5 the mean square radius of bubbles growing in 0·2 mol dm^{-3} CO_2 solutions is plotted against time. For the glycerol-containing solution the plot is linear with a gradient of $1{\cdot}5 \times 10^{-7}$ m^2 s^{-1} but with no glycerol present the plot, which has an initial gradient of $3{\cdot}7 \times 10^{-7}$ m^2 s^{-1}, deviates from linearity at the later times. The corresponding values of g are $2{\cdot}7 \times 10^{-9}$ and $7{\cdot}0 \times 10^{-9}$ m^5 mol^{-1} s^{-1} respectively, with a ratio of 0·4, which is comparable with an expected value of 0·5 based on the theoretical inverse relationship between the diffusion coefficient of solute molecules and the solution viscosity.

Bubble formation

In seeking a plausible mechanism to explain the origin of the bubbles formed in the reaction cell, we first consider the effect of hydrophobising the cell by coating its internal surface with perfluorinated polymer. As Fig. 6 shows, this treatment produces a superabundance of bubbles, with the rate of increase in bubble number versus supersaturation being much greater than for the untreated cell. Extrapolation of the data to zero bubble formation in the latter case indicates a critical supersaturation of about 3. Extrapolation is more uncertain for the hydrophobised cell, but the critical supersaturation appears to be closer to 1.

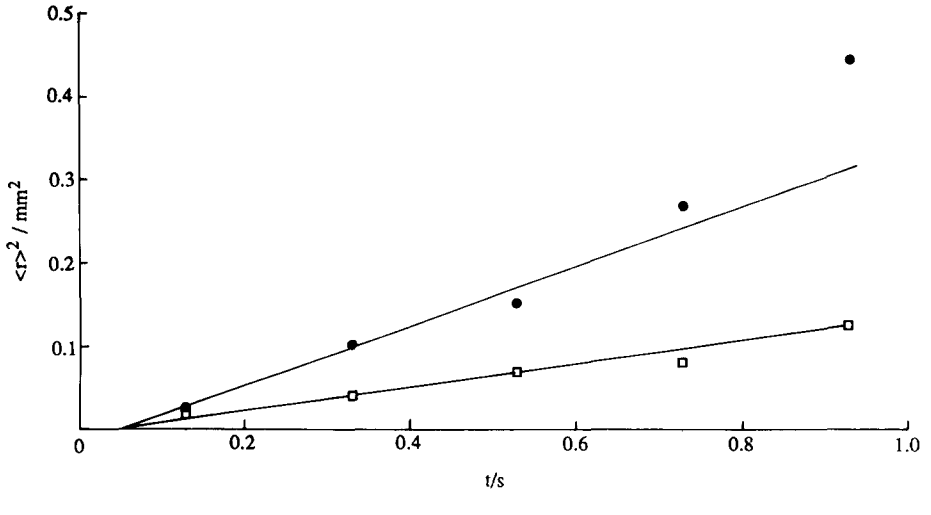

Fig. 5. Time dependence of mean square bubble radius obtained from video recordings of solutions with initial CO_2 concentrations of 0·2 mol dm^{-3}: (●) no added glycerol, (□) 25% added glycerol.

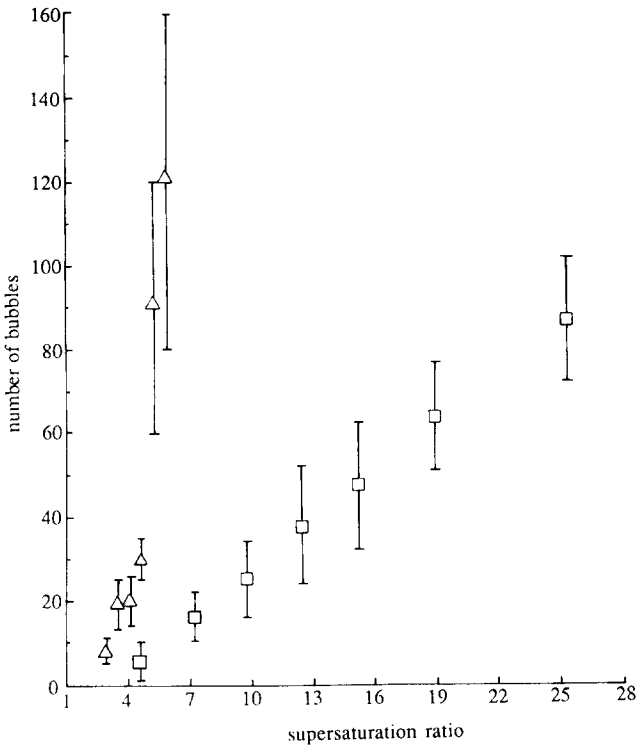

Fig. 6. Number of CO_2 gas bubbles/cm^3 of solution at t = 130 ms plotted against supersaturation ratio: (□) untreated cell + 25% added glycerol, (Δ) hydrophobised cell + 25% glycerol. Error bars indicate standard deviations.

To characterise the nature of the treated surface, measurements were made of the contact angles of NaCl solutions against tilted glass microscope slides which had been subjected to the same cleaning and hydrophobising procedure used for the cell. The results revealed that the advancing contact angle was virtually constant but that the receding angle decreased markedly as the tilt angle was increased (Fig. 7). For rigorously cleaned surfaces this contact angle hysteresis is characteristic of surface roughness.

Before rationalising these observations we first refer to some calculations of nucleation rates in aqueous solutions of CO_2 at 298 K for a supersaturation of about 5 (Wilt, 1986). Classical nucleation theory was used to predict that neither homogeneous nor heterogeneous nucleation on surfaces which are smooth planar or which contain conical or spherical projections can occur. For large contact angles, heterogeneous nucleation is predicted from conical cavities with sufficiently narrow cone angles (e.g. for θ = 94° the required cone angle is about 10°). Results for spherical cavities were inconclusive, but in a further paper, Ciholas and Wilt (1988) state that spherical cavities small enough to become nucleation sites cannot be treated by classical nucleation theory.

A recent experimental study of aqueous solutions which were supersaturated with 50 atm N_2 gas has confirmed that bubble formation is not facilitated by smooth surfaces, whether hydrophilic or hydrophobic (Ryan & Hemmingsen, 1993). In contrast to this behaviour it is a commonplace observation that rough surfaces are often very effective in initiating bubble formation, e.g. when naturally carbonated mineral water is pumped through pipes with rough surfaces CO_2 gas is evolved (Fox, 1988).

In most cases, the mechanism of bubble formation on rough surfaces is unlikely to be *de novo* nucleation from conical cavities since unusually large contact

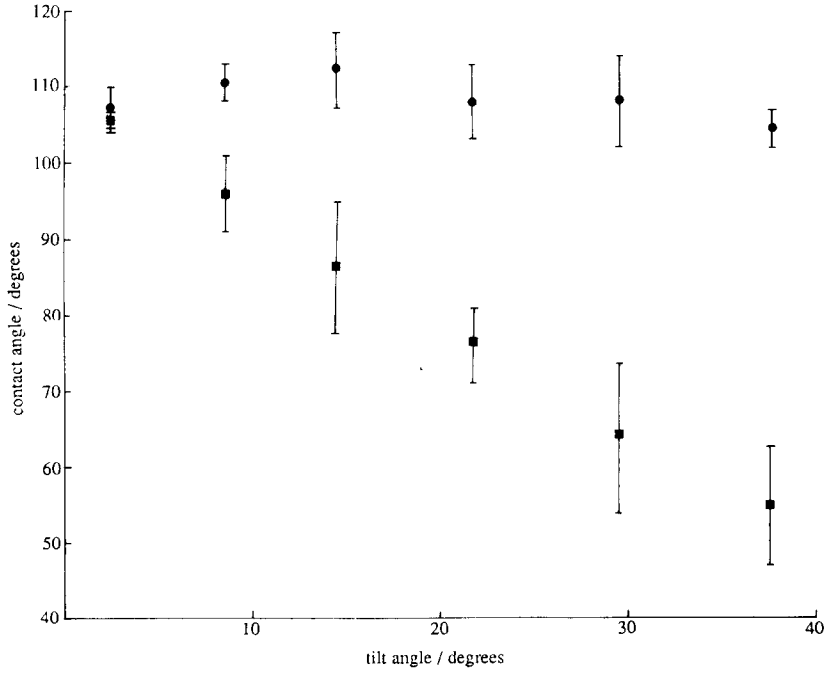

Fig. 7. (●) Advancing and (■) receding contact angles for 0·15 mol dm^{-3} NaCl solution on hydrophobised glass microscope slides. Error bars indicate standard deviations.

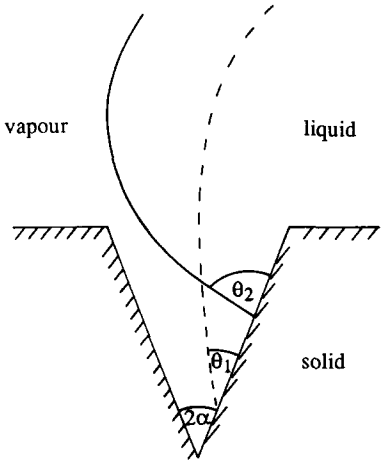

Fig. 8. Schematic representation of gas entrapment in a crevice by an advancing liquid surface.

angles are required. A more probable explanation is that tiny pockets of gas held at the surface act as nuclei (Newton Harvey *et al.*, 1944). Most real solid surfaces will contain pits, scratches and other irregularities and if the surface is not completely wetted by the liquid, some of these cavities may be expected to contain trapped gas. The mechanism of entrapment is illustrated in Fig. 8 for a liquid front advancing over a gas-filled groove. Because of the convex shape of the liquid surface, the advancing liquid with contact angle θ_2 will strike the opposite wall of the cavity before the contact line reaches the bottom of the groove. The liquid front with contact angle θ_1, on the other hand, will advance to fill the cavity completely. Since the requirement for gas entrapment is $\theta_a > 2\alpha$, where θ_a represents the advancing contact angle, and 2α the cone angle, hydrophobic surfaces should contain many more trapped gas pockets than hydrophilic surfaces.

For a cavity containing trapped gas to be active as a nucleation site, the supersaturation must be above a critical value to cause the gas to expand out of the cavity to form a detached bubble. This critical value can be related to the size of an idealised conical cavity with a mouth radius R and a cone angle of 2α if the gas/liquid interface is assumed to be part of a spherical surface of radius r. Figure 9 shows the manner in which the liquid profile changes as the gas volume increases (Cole, 1974). For contact angles satisfying the condition $2\alpha < \theta \leq 90°$ (Fig. 9(a)), r first increases as the interface moves up the cavity. However, as the contact line turns the corner at the mouth of the cavity, r decreases and then begins to increase again. As a result, R/r decreases initially and then increases to a maximum value of 1 as the interface emerges from the cavity. At higher contact angles the interface may be concave initially (Fig. 9(b)), when the radius of curvature is defined to be negative. As the gas volume increases, the interface becomes flatter until, as the contact line reaches the mouth of the cavity, the curvature reverses

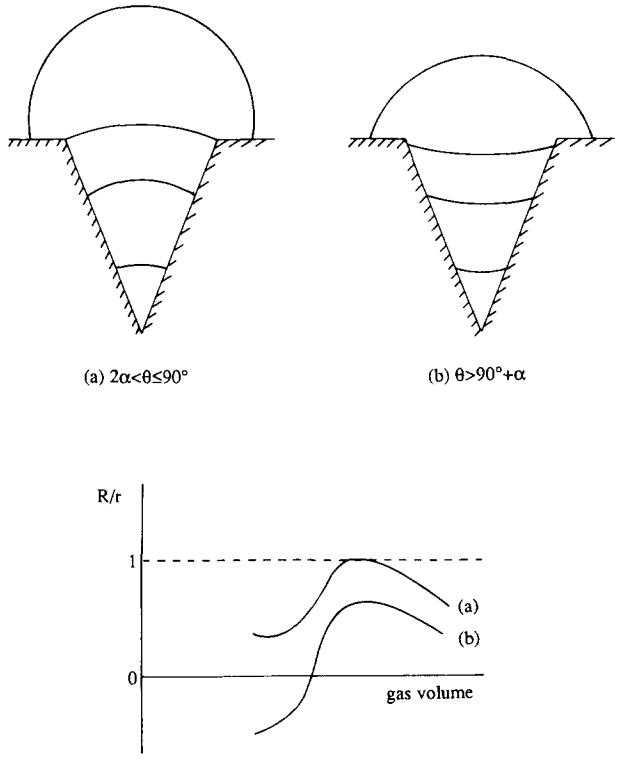

Fig. 9. Variation in the radius of curvature (r) of a gas bubble as it increases in volume and grows out of a conical pit with a mouth radius R.

and R/r changes sign. On further growth R/r passes through a maximum value which approaches 1. Thus, over a significant range of contact angles, r has a minimum value approximately equal to R. For a gas bubble in equilibrium, a minimum in r corresponds to a maximum in the pressure difference across the interface according to the Young–Laplace equation:

$$\Delta P = \frac{2\gamma}{r} \tag{8}$$

where γ is the surface tension. If an emergent bubble is to continue growing therefore, the supersaturation must be equivalent to a gas pressure which exceeds $2\gamma/R$.

The effects of changing contact angle and supersaturation on bubble formation shown in Fig. 6 can now be explained on the basis of pre-existing gas cells. In our model the increase in the number of bubbles from the hydrophobic surface is attributed to an increased number of trapped gas cells while the increase with supersaturation reflects the activation of cavities with decreasing exit radii. Equation (8) can be used to estimate the maximum size of gas-filled cavity in the surface from the critical supersaturation of 3 found in the hydrophobic cell. By putting the excess pressure in the bubble (ΔP) equal to 2×10^5 N m^{-2} and γ equal to 72 mN m^{-1}, a value of 0·7 μm is obtained for r. The lower critical supersaturation indicated for the treated cell implies that larger cavities are active as nucleation sites on the hydrophobic surface.

Table 1. Effect of sodium dodecyl sulphate (SDS) on the number of CO_2 gas bubbles/cm^3 present in the reaction cell 130 ms after supersaturation of 4·62 was established in 0·15 mol dm^{-3} NaCl solutions

[SDS] (mM)	γ (mN m^{-1})	Hydrophilic surface		Hydrophobic surface	
		θ (deg)	N (cm^{-3})	θ (deg)	N (cm^{-3})
0	71·9	33 ± 9	8 ± 2	107 ± 2	373 ± 91
0·208	66·8	28 ± 5	2	92 ± 6	172 ± 50
0·415	45·4	26 ± 5	3	88 ± 5	119 ± 30
0·830	37·8	18 ± 5	14 ± 1	79 ± 6	61 ± 15
1·660	35·3	14 ± 5	49 ± 12	74 ± 9	86 ± 19

SDS concentrations below the dashed line exceed the critical micelle concentration. Contact angles (θ) were measured against glass microscope slides. Error limits represent standard deviations.

As a further check on the model, the effect of altering the contact angle (θ) by the addition of sodium dodecyl sulphate (SDS) was investigated. Results are summarised in Table 1 where the quoted value of θ represents an extrapolation of advancing and receding angles to zero tilt. It can be seen that whilst θ on the hydrophilic surface is practically unaffected by the addition of SDS, on the hydrophobic surface it is initially reduced at low SDS concentrations. As expected, there is a correlation between θ and the number of bubbles observed, with fewer bubbles being formed as θ decreases. However, at higher SDS concentrations the number of bubbles begins to rise again, although θ remains virtually constant. This phenomenon occurs with solutions whose surface tensions have reached a constant value, indicating that the SDS concentrations are above the critical micelle concentration and that SDS micelles can act as nucleation sites for bubble formation.

Finally, a few measurements were carried out in which protein was adsorbed onto the hydrophobic cell surface. Two proteins were chosen for study: β-casein, which is a disordered protein with pI = 5·2 and β-lactoglobulin which is a globular protein with pI = 5·1. Both proteins lowered the contact angle and inhibited bubble formation. The data (including standard deviations) were as follows: β-casein, $\theta = 53 \pm 10°$, $N = 137 \pm 39$ cm^{-3}; β-lactoglobulin, $\theta = 77 \pm 10°$, $N = 447 \pm 77$ cm^{-3}. A comparison of the results for the two proteins shows that the number of bubbles correlates with θ in the same way as for the SDS data.

CONCLUSIONS

Turbidimetric measurements together with analysis of photographic and videorecorder images show that carbon dioxide bubbles formed in aqueous solution by the reaction between hydrochloric acid and sodium bicarbonate grow at a rate which is diffusion-controlled. At supersaturations typical of carbonated beverages, bubble formation in the glass stopped-flow apparatus originated at the walls of the reaction cell where the nucleation sites were probably pre-existing pockets of trapped gas. When the surface of the cell was hydrophobised by the adsorption of a perfluorinated polymer, bubble formation was greatly enhanced. The effect of adsorbing sodium dodecyl sulphate, β-casein or β-lactoglobulin onto the hydrophobic surface is to reduce the number of bubbles formed. SDS micelles appear to act as nucleation centres.

In the context of the technology associated with the production of carbonated beverages, it is concluded that the surface properties of the container are extremely important in determining the number of bubbles which form in a solution after critical supersaturation is exceeded. The results suggest that by modifying the wetting characteristics of containers, some control over the extent of bubble release might be achievable.

ACKNOWLEDGEMENTS

The authors gratefully acknowledge the assistance of Mr J. Eyett in setting up the photographic equipment and the help given by Mr D. Ferdinando with the analysis of the Quantimet data. A. M. H. thanks the Agricultural and Food Research Council for the award of a Co-operative Studentship sponsored by Unilever Research.

REFERENCES

Cable, M. & Frade, J. R. (1988). The influence of surface tension on the diffusion-controlled growth or dissolution of spherical gas bubbles. *Proc. R. Soc. Lond.*, **A420**, 247–67.

Ciholas, P. A. & Wilt, P. M. (1988). Nucleation rates in water–carbon dioxide solutions: the spherical cavity case. *J. Coll. Interface Sci.*, **123**, 296–8.

Cole, R. (1974). Boiling nucleation. *Adv. Heat Transfer*, **10**, 85–167.

Epstein, P. S. & Plesset, M. S. (1950). On the stability of gas bubbles in liquid–gas solutions. *J. Chem. Phys.*, **18**, 1505–9.

Fogg, P. G. T. & Gerrard, W. (1991). *Solubility of Gases in Liquids: A Critical Evaluation of Gas/Liquid Systems in Theory and Practice*. John Wiley, Chichester, Ch. 11.

Fox, B. (1988). Secrets of the source. *New Scientist*, 19 November 1988, 45–8.

Gibbons, B. H. & Edsall, J. T. (1963). Rate of hydration of carbon dioxide and dehydration of carbonic acid at 25°C. *J. Biol. Chem.*, **238**, 3502–7.

Hilton, A. M., Hey M. J. & Bee, R. D. (1993). Nucleation and growth of carbon dioxide gas bubbles. In *Food Colloids and Polymers: Stability and Mechanical Properties*, ed. E. Dickinson & P. Walstra. Royal Society of Chemistry Special Publication No. 113, Cambridge, pp. 365–75.

Lothian, G. F. & Chappel, F. P. (1951). The transmission of light through suspensions. *J. Appl. Chem.*, **1**, 475–82.

Lubetkin, S. D. (1989). The nucleation and detachment of bubbles. *J. Chem. Soc., Faraday Trans.*, **I, 85**, 1753–64.

Luey, J.-K., McGuire, J. & Sproull, R. D. (1991). The effect of pH and NaCl concentration on adsorption of β-lactoglobulin at hydrophilic and hydrophobic silicon surfaces. *J. Coll. Interface Sci.*, **143**, 489–500.

Manley, D. M. J. P. (1960). Change of size of air bubbles in water containing a small dissolved air content. *Brit. J. Appl. Phys.*, **11**, 38–42.

Newton Harvey, E., Barnes, D. K., McElroy, W. D., Whiteley, A. H., Pease, D. C. & Cooper, K. W. (1944). Bubble formation in animals. I. Physical factors. *J. Cell. Comp. Physiol.*, **24**, 1–22.

Ryan, W. L. & Hemmingsen, E. A. (1993). Bubble formation in water at smooth hydrophobic surfaces. *J. Coll. Interface Sci.*, **157**, 312–17.

Sugden, S. (1924). The determination of surface tension from the maximum pressure in bubbles, Part 2. *J. Chem. Soc.*, **125**, 27–31.

Wilt, P. M. (1986). Nucleation rates and bubble stability in water–carbon dioxide solutions. *J. Coll. Interface Sci.*, **112**, 530–8.